Available online at www.sciencedirect.com
SCIENCE DIRECT®
Journal of Power Sources 133 (2004) 229–242
JOURNAL OF POWER SOURCES
www.elsevier.com/locate/jpowsour

Materials prepared for lithium ion batteries by mechanochemical methods

L.J. Ning [a], Y.P. Wu [a,b,1], S.B. Fang [a], E. Rahm [b], R. Holze [b,*]

[a] *Institute of Chemistry, Chinese Academy of Sciences, Beijing 100080, China*
[b] *Technische Universität Chemnitz, Institut für Chemie, AG Elektrochemie, 09107 Chemnitz, Germany*

Received 16 July 2003; accepted 28 January 2004

Available online 9 April 2004

Abstract

Since the birth of the lithium ion battery in the early 1990s a lot of methods has been tried to prepare materials with better performance and/or lower cost. In comparison with other methods, mechanochemical methods are advantageous because they are based on simple processes, show high efficiency, low energy consumption and cost They are widely applied to prepare materials for lithium ion batteries such as cathode materials, anodic ones and solid electrolytes. The latest progress on these aspects is reviewed in this paper including the effects of mechanochemical methods and mechanisms in improving electrochemical performance. In addition, some problems concerning some materials and further directions are pointed out.

Keywords: Lithium ion battery; Mechanochemical methods; Cathode materials; Anode materials; Electrolytes

1. Introduction

A mechanochemical method effects a chemical reaction via mechanical ways. These methods comprise numerous different processes, especially grinding and milling such as ball milling, colloidal milling, and jet milling. During milling or grinding, mechanical energy is transferred to the particles of reactants and causes a lot of changes such as deformation, friction, fracture, amorphization, quenching, and so on. Later, new product phase(s) at the interfaces of the reactants is(are) formed. With diffusion of atoms of the reactant phases, which constitute a barrier layer preventing further reaction, the product phase grows further and the chemical reaction is realized [1]. The main advantage is its simplicity in the synthetic process, effective mixing accompanying a break-off of chemical bondages and their re-combination, and decrease in energy expenses as well as the cost of the materials. It has been widely applied in inorganic and organic synthesis, metallurgy (new method of mechanical alloying of metals), the production of ceramics, ferrites, ferroelectrics, mineral fertilizers, and construction materials, activation of catalysts, and pharmaceutical industry [2]. Of course, it has some limitation, for example, it usually leaves defects such as dislocations and could not prepare components with ideal crystal structure.

The mechanochemical methods have long been associated with the birth of lithium ion batteries, but this has been ignored or not completely realized. For example, the preparation of cathode materials of lithium cobalt oxides ($LiCoO_2$) at first adopted the mechanochemical method to mix fully salts and/or oxides of lithium and cobalt, followed by a heat-treatment or calcination [3]. In this way, the calcination time at high temperature ($\geq$800 °C) will be shortened. If other methods are adopted, they will take more time and consume more energy. In addition they might not yield the same products and properties as obtained via mechanochemical methods.

Since the development of lithium ion batteries has been very rapid [3], the competition becomes more and more drastic, and materials with higher performance and/or lower cost are greatly desired. Recently, a lot of methods has been widely explored such as incorporation of heteroatoms [4], composite technology [5,6], soft-chemistry routes [7], some non-classic methods such as template methods, pulsed laser deposition, plasma-enhanced chemical vapor deposition, radio-frequency magnetron sputtering [8], and sol–gel methods [9] to prepare materials for lithium ion batteries.

* Corresponding author. Tel.: +49-371-5311-509; fax: +49-371-5311-832.
E-mail addresses: wuyp@fudan.edu.cn (Y.P. Wu), rudolf.holze@chemie.tu-chemnitz.de (R. Holze).
[1] Present address: Department of Chemistry, Fudan University, Shanghai 200433, China.

0378-7753/$ – see front matter © 2004 Elsevier B.V. All rights reserved.
doi:10.1016/j.jpowsour.2004.01.048

Of course, mechanochemical methods have also been tried. In this paper, the latest progress on this aspect is primarily reviewed. Some simple processes will not be included here. The prepared materials for lithium ion batteries by mechanochemical methods include cathode materials, anode materials and solid electrolytes.

2. Cathode materials

There are several kinds of cathode materials such as lithium cobalt oxides, lithium nickel oxides, lithium manganese oxides ($LiMn_2O_4$) and vanadium oxides. Of course, all of them have been prepared by mechanochemical methods. Lithium cobalt oxides, spinel lithium manganese oxides, and other kinds of cathode materials will be mainly reviewed.

2.1. Lithium cobalt oxides

As early as 1987, it was reported that a layered phase related to $LiCoO_2$ was achieved by mechanochemical methods by ball-milling mixtures of lithium and cobalt hydroxides [10]. However, since the mobility of lithium is increased by mechanical activation, spinel Co_3O_4 appears after milling for longer time, and its electrochemical performance could not be satisfactory.

The reaction during ball milling of $LiOH{\cdot}H_2O$ and $Co(OH)_2$ powders is different from the heat-treatment process. $Co(OH)_2$ decomposes at first into CoOOH, and then reacts with LiOH to form $LiCoO_2$ [11]. Consequently, CoOOH and LiOH can be used to prepare $LiCoO_2$ with a cubic spinel-related structure by ball milling at a shorter time [12]. Followed by firing at 600 °C for 2 h, highly crystallized $LiCoO_2$ similar to HT-$LiCoO_2$ prepared at high temperature (≥800 °C) with a cubic structure is obtained [11]. If the ratio of ball to powder weight is increased, the mechanochemical reaction will be enhanced due to increased number of collisions and more absorbed collision energy per particle.

$LiCoO_2$ prepared by a mechanical activation in an AGO-2 planetary activator with water cooling is characterized by high dispersion, structural disorder, and different electronic states of transition metal ions [13,14]. As a result, the prepared $LiCoO_2$ does not show good electrochemical performance. In combination with subsequent firing or heat-treatment at 850 °C, well-ordered $LiCoO_2$ can be prepared with good electrochemical performance. This mechanochemical treatment can decrease the heat-treatment temperature to achieve crystal structure and shorten heat-treatment time [15].

However, if crystal $LiCoO_2$ from high temperature treatment by sol–gel methods or solid-state reaction is processed by ball milling, it will transform from hexagonal to cubic structure, indicating transformation into a disordered rock-salt structure and larger lattice constants. The effects are caused by loss of lithia (Li_2O) and oxygen to form $Li_xM_{1-x}O$ ($0.25 \leq x \leq 0.5$), an unwelcome phase resulting in poor electrochemical performance [16]. These observations and results are summarized in Table 1.

2.2. Spinel lithium manganese oxides ($LiMn_2O_4$)

There are several kinds of lithium manganese oxides [3,17]. Applied in lithium ion batteries, the spinel $LiMn_2O_4$ is the most promising one.

Mechanochemical methods can be used to synthesize highly dispersed $LiMn_2O_4$ spinel starting from different manganese (MnO_2, Mn_2O_3, MnO) and lithium (Li_2O, LiOH, $LiOH{\cdot}H_2O$, Li_2CO_3) compounds [14,18–21]. The oxidation state of manganese greatly influences the kinetics of mechanochemical reactions. For example, MnO_2 reacts almost completely with Li_2CO_3 to produce $LiMn_2O_4$, but no observable interaction between Mn_2O_3 and MnO with Li_2CO_3 occurs. On the other hand, different crystal structures and mechanical properties of initial lithium compounds result in different mechanisms of mechanochemical action of the activated mixtures. LiOH has a layered structure and exhibits good plasticity, and the chemical interaction during mechanochemical processing between MnO_2 and LiOH is preceded by the stage of the molecular-dense aggregates (mechanocomposites) formation under action of the adhesion forces, and the surface of the mechanocomposites is covered by the amorphous LiOH layer. In the case of Li_2CO_3, it is a typical ionic compound and more brittle, and a process of brittle fracture of the components of MnO_2 and Li_2CO_3 proceeds [19]. Furthermore, milling time presents different effects on charge and discharge curves since mechanical energy can be comparable with treatment at high temperature. At intermediate milling

Table 1
Selected results of $LiCoO_2$ prepared by mechanochemical processes

Raw materials	Process	Features of structure	Electrochemical performance	References
$LiOH + Co(OH)_2$	Milling/10 h	HT-$LiCoO_2$	–	[10]
$LiOH + Co(OH)_2$	Milling/40 h	HT-$LiCoO_2$ + spinel Co_3O_4	–	[10]
$LiOH{\cdot}H_2O + Co(OH)_2$	Ball milling + 600 °C/2 h	$LiCoO_2$	–	[11]
$LiOH + Co(OH)_2(Co(OH)_2)$	Milling + 600 °C/4 h	Disordered, dispersed HT-$LiCoO_2$	Medium	[12]
$Li_2O + CoO$	Milling	Spinel $LiCoO_2$	Poor	[13]
$LiOH{\cdot}H_2O + Co(OH)_2$	Ball milling + 850 °C/24 h	HT-$LiCoO_2$	Good	[15]
HT-$LiCoO_2$	Ball milling	$LiCoO_2$ + disordered $Li_xM_{1-x}O$	Poor	[16]

time, the prepared spinel $LiMn_2O_4$ shows a typical charge and discharge curves of spinel $LiMn_2O_4$ prepared at high temperature, i.e. two plateaus at 3 and 4 V. Longer milling time results in amorphization and decomposition the spinel $LiMn_2O_4$ into Mn_2O_3 [21].

The spinel $LiMn_2O_4$ obtained from the mixture of Li_2O and MnO_2 is highly disordered nanocrystalline with particle size less than 25 nm and has much strain variances or defects [14,20,21]. The intercalation of Li^+ takes place with an initial capacity of 167 mAh/g in the 2.5–4.3 V range with a steady slope instead of two plateaus at the around of 4 and 3 V. Due to the existence of the highly disordered structure, which could accommodate the Jahn-Teller distortion of the spinel structure during Li^+ intercalation in the 3 V region [3,17] and the fine nanoparticles of the powder, it shows better capacity retention as compared to well-ordered crystalline $LiMn_2O_4$ powders [20]. Of course, the polarization is also greatly decreased.

In addition, nonstoichiometric $Li_xMn_2O_4$ ($x > 1$) spinels can also be prepared by mechanochemical activation [19]. The composition and lattice constants of the final products are affected by lithium content. The intergrain resistance rather than the bulk properties of the spinels, including starting reagents and the molding pressure, determines their conductivity. For example, nonstoichiometric $Li_xMn_2O_4$ from Li_2CO_3 has higher conductivity than that from LiOH. The activation energy of conductivity (E_a) does not depend on x over a wide composition range $0.21 \leq x \leq 1.21$, and is 0.36 ± 0.04 eV [19]. Of course, it is also comprised of disordered nanocrystallines. Furthermore, Li doping increases the valence of Mn above 3.5 [2]. As a result, the prepared nonstoichiometric $Li_xMn_2O_4$ ($x > 1$) spinel will also be more stable in cycling.

Of course, modification of cathode materials can also be done by mechanochemical methods. When $LiMn_2O_4$ from a solid-state reaction or a sol–gel method is ball-milled for a sufficient time [22,23], a nano $LiMn_2O_4$ with excellent capacity retention in the 3 V range at room temperature will be achieved. During ball milling the particles are broken into nanoparticles that are stuck back together as hard agglomerates, and many nanograins (20–40 nm) are generated within a big crystallite by the action of defects such as dislocation and strain at grain boundaries. By the way, partial oxidation of manganese ions also happens [22]. Of course, the Jahn-Teller effect associated with the spinel structure still exists during lithium deintercalation and intercalation. However, the net deformation of a particle with small grains is less anisotropic than of a particle with large grains and there is less possibility of fracture of particles due to the tetragonal distortion. Furthermore, the strain imposed by the formation of the tetragonal phase is expected to be accommodated by the already existing strain in particles. By the way, the ball milling provides intimate mixing improving the electrical contact between spinel particles and carbon. As a result, the Jahn-Teller distortion is greatly alleviated, and the cycling behavior is much improved [23]. As shown in Fig. 1, in a 50-cycle test with 0.5 mA/cm^2, a sample ball-milled for 1 h gives a constant capacity of 122 mAh/g between 2.4 and 3.4 V versus lithium and the cycling behavior at elevated temperatures is also satisfactory. Some selected results are summarized in Table 2.

In summary, compared with conventional solid-state processes, the mechanochemical methods appear to accelerate and simplify the synthesis process, and decrease the energy expenses as well as the cost of the material [14]. Consequently, based on the favorable doping [2], other kinds of heteroatoms can also be added to prepare doped spinel $LiMn_2O_4$, and further improvement will be achieved. Furthermore, it can be combined with other methods such as high temperature heat-treatment, and different $LiMn_2O_4$ spinels can be prepared [24].

2.3. Other cathode materials

Other kinds of cathode materials such as $Li_{1+x}V_3O_8$ [14], $LiMO_2$ (M = Ti, Ni, Mn and Fe) can also be prepared by ball-milling mixtures of lithium and transition metal oxides. However, the resulting oxides except $LiMnO_2$ have the rock-salt structure with the transition metal and lithium ions randomly ordered in the cation sites, and the electrochemical performance of the milled samples as cathodes in lithium batteries is poor, presumably due to the disorder of the cation lattice [16]. In the case of $LiMnO_2$, the short-range cation order still exists even after extended milling, and

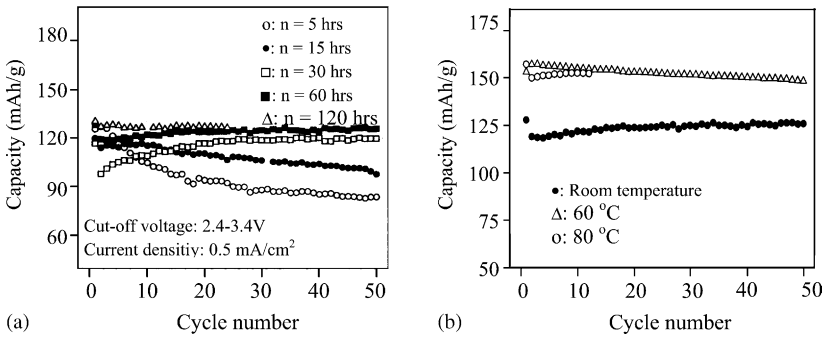

Fig. 1. Effects of ball-milling time on (a) cycling behavior of $LiMn_2O_4$ and (b) cycling behavior of one $LiMn_2O_4$ sample after 1 h milling at different temperature: voltage range of 2.4–3.4 V, current density of 0.5 mA/cm^2 (from ref. [22]).

Table 2
Selected results of $LiMn_2O_4$ prepared by mechanochemical processes

Raw materials	Process	Features of structure	Electrochemical performance	References
$LiOH(LiOH{\cdot}H_2O, Li_2CO_3) + MnO_2$	Milling	Nanocrystallie $LiMn_2O_4$	4 V, good	[19]
$LiOH + Mn_2O_3$ (MnO)	Milling	No $LiMn_2O_4$	–	[19]
$Li_2O + MnO_2$	Grinding	Disordered nano spinel $LiMn_2O_4$ with strain or defects	3 V, 4 V plateaus, good cycling	[20,21]
$LiMn_2O_4$ from solid-state reaction	Ball milling	Nanodomains, strains, defects	3 V, good cycling	[23]

it presents good electrochemical performance [16]. In addition, extensive milling of a rhombohedral $Li_3Fe_2(PO_4)_3$ (NASICON-type structure) from ion exchange can improve its electrochemical performance, and more lithium can be inserted as compared with mild milling [25].

3. Anode materials

There are various kinds of anode materials such as carbonaceous materials, alloy-based anode materials etc. [3]. Some of them have been prepared or modified by mechanochemical methods, and they present some interesting properties.

3.1. Carbonaceous materials

Carbonaceous materials are the first available and dominant ones one the market. Since the highest reversible capacity of graphite is 372 mAh/g, a lot of methods has been tried to break through this limit such as doping with heteroatoms [2,26]. Recently, it was found that milling or grinding is a good way to modify electrochemical performance of carbon materials, and there are several ways such as ball milling, turbo milling, jet milling and colloidal milling. Their effects on carbonaceous materials are mainly related into structure and electrochemical performance as shown in Table 3.

3.1.1. Structural changes after milling

The structure of carbonaceous materials changes with ball-milling period and mode. These changes mainly include the following aspects as shown in Table 3: particle size, surface area, surface structure, electronic self-spinning of radicals, microstructure such as defects and nanocavities or voids, and crystal structure.

After milling, the graphite particle size will change. In general, bond-breaking of graphene layers leads to smaller particles [27]. For example, after 150 h of ball milling, the well-graphitized graphite is pulverized into small particles with a size of about 50 nm. Due to the large surface energy, the merging of single particles is favored and results in the formation of agglomerates with average size about 1 μm [28]. In the case of impact/shock type of ball milling, the interactions vertical to the graphite cleavage planes are so strong that graphite particles are torn into pieces of disordered carbons. Though jet milling and turbo milling are soft and mild techniques, they also cut graphite particle into smaller ones in the direction both perpendicular and parallel to the basal planes [29].

Since the particle size becomes smaller, its specific surface area increases with milling though the degree depends on the milling mode [27,30–32].

Surface structure and especially the composition of surface groups are greatly changed. Different atmospheres including air, highly pure argon, nitrogen and CO_2 result in different effects. The active surface sites formed by milling react readily with active gases like e.g. O_2, CO_2, and H_2O to produce oxygen-containing highly reactive surface groups [33]. Reactive milling can be used to develop bonding between carbon and lithium atoms, and form a lithiated surface [34].

ESR spectra of natural graphite powder vary with grinding methods. The linewidth due to conduction electron spins broadens for specimens except that ground by a ball-mill down to 1 μm diameter. The contribution of localized spins produced in the mechanical grinding process becomes predominant over that of conduction electron spins in the range of $T < 50$ K [35]. On the other hand, the absorption of ball-milled material satisfies the Curie law. Samples ground by jet-milling have large g-values as compared with those prepared by ball and colloidal milling. In the magnetic field, due to anisotropy of the diamagnetic susceptibility, particles rotate for the jet-milling with the largest diameter of 100 μm [36]. However, for each grinding mode, the change is totally independent of the nature of the used precursors (graphite, carbon, coke) and/or of its morphology (layers, microbeads and fibers) [35].

Microstructure is also affected by the mechanochemical treatment. For example, shock type mechanical milling generates a large ratio of disorder within the powder, and small stacks of 2–3 parallel fringes less than 1 nm comprised of small coherent domains. These disordered domains are misoriented and distributed at random to form mesopores, and no single layer is observed. The shear-type grinding generates a weaker mechanical strain than the shock mode, and samples are much less damaged with less defects in the direction both perpendicular and parallel to the basal planes [29]. Depending on the type of grinding, energetic interactions of different intensity are generated allowing for disordering or disorganization of the carbonaceous materials [27,30,37], which has been observed by transmission electron microscopy [32,37] and includes a lot of vacancies,

Table 3
Selected results of the effects of mechano-chemical methods on structure and electrochemical performance of graphite

Factors of mechano-chemical methods	Features of the factors	Changes of structure parameters						Electrochemical performance	References
		Particle	Surface area	Surface structure	Radicals	Microstructure	Crystal structure		
Jet- and turbo-milling	Soft, mild	Cut into smaller	Increase		Localized spins, larger g-value		Little change in d_{002}, decrease in L_c	Decrease in irreversible capacity, increase in coulomb efficiency under optimal condition	[29,35,36]
Ball- and colloid milling		Nanometer, agglomerates	Increase		Localized spins, smaller g-value		Increase or little change in d_{002}, and decrease in content of hexagonal phase	Increase in reversible capacity and coulomb efficiency, improved cycling	[28,30,36]
Impact/shock-type mechanical milling/grinding	Drastic, strong	Torn into pieces of disordered carbon	Increase	O-terminated carbon		Large ratio of disorder such as vacancies, microcavities, and voids	Decrease of L_a and L_c,	Increased reversible capacity mainly associated with the charge slope >1.0 V, increase of irreversible capacity, capacity fading	[27,29,35,37]
Shear-type grinding	Shear force		No evident change	O-terminated carbon		Less disorder or disorganization such as vacancies, microcavities	Little change in crystal size and d_{002}	Increase in reversible and irreversible capacity	[35,37]
Reactive milling	Graphite + lithium		Increase	Lithiated surface				Spontaneous formation of surface passivating film, high reversible capacity, lower hysteresis	[34,45]
Reactive atmosphere	Such as O_2, CO_2, H_2O		Slight increase	Oxygen-containing groups		Disorder present	Little change of d_{002} and crystal size	Loose surface passivating film, exfoliation of graphite, capacity fading, slight increase of reversible capacity	[32,33]

microcavities or voids and metastable carbon interstitial phases with sizes around 1.3 nm, which are formed among the agglomerated particles [28,31].

Different atmospheres also present different microstructure. For example, in the case of ball milling in a planetary mill where the deformation forces are mainly shear in nature, mechanically induced oxidation on the surface, probably along the edges of the graphene planes, suppresses the fracture rate and preserves the crystallinity of natural graphite milled in oxygen [38].

Generally, after milling, the crystal structure of carbonaceous materials will also be changed and this is mainly reflected in disordering of structure, and the changes in the interlayer distance, d_{002}, and the content of crystal phases [3,27,29,30]. d_{002} usually increases with milling time due to the introduction of voids and vacancies. However, in the case of mild milling such as turbo and jet milling, little change in d_{002} of the material is observed due to less destructive effect on graphite particles [29]. The graphite lattices become thinner due to expansion of graphite-layer interspacing [27]. As a result, the content of hexagonal phase decreases and that of rhombohedral increases [3]. However, there is a contradicting report that the rhombohedral phase fraction decreases with milling time and then stabilizes at about 10% [30]. Perhaps it depends on the species of graphite.

In the case of other kinds of carbons such as nongraphitic carbon, the milling also affects the particle size distribution, BET specific surface area, interlayer distance and other structures [31,39].

3.1.2. Electrochemical change after milling

As mentioned above, different changes in structures have been observed resulting from different milling conditions. As a result, electrochemical performance also changes greatly, and some selected results are shown in Table 3.

In the case of graphite after milling, the reversible capacity is increased, up to 700 mAh/g [28,35,37,40,41]. Of course, this increase is dependent on the type or mode of milling and milling time, and is due to several aspects: (1) the production of a large amount of edge planes during milling, which are highly active and react with lithium [40]; (2) vacancies, microcavities or voids and interstitial phase at the edges of the metastable carbon, where lithium can dope [28,37,42]; and (3) other present disorder structures [32]. By the way, the particle size also influences the initial charge capacity as shown in Table 4 [43,44]. When it is smaller, more inlets and outlets for lithium on the surface of graphite crystallites and edge planes are provided. As a result, reversible lithium capacity is increased, above the theoretic value of graphite.

Since considerable defects and disordering are introduced into the milled graphite, a high reversible capacity is usually accompanied with a large irreversible capacity. For example, a graphite after 80 h of shock-grinding is able to reversibly intercalate two lithiums per six carbons 'Li_2C_6' while still having an irreversible capacity of 0.8 Li, 320 mAh/g [35,41]. Active structures such as the large amount of edge planes [40], vacancies, microcavities or voids and interstitial phases at the edges of the metastable carbon [28,37,42] are the main contribution to irreversible capacity. Of course, the increased surface area also contributes to irreversible capacity since the surface is more susceptible to irreversible reactions in the first cycle [32].

It is usually observed that the enhanced capacity is associated with a pronounced charge potential hysteresis at >1.0 V [28,32,37]. During charge–discharge cycles, the reversible capacity above 1 V decreases rapidly [42]. Another report says that the charge slope at >1.0 V, converts to a plateau at <0.25 V after repeated cycling or additional heat-treatment at 1000 °C, suggesting the disordered structure can transform into a more ordered graphitic one upon cycling or heat-treatment [28]. This voltage hysteresis at >1.0 V during charging results most likely from the disordered surface structure formed during the milling process [28,37] and the bonding change between the interstitial carbon and the carbon in the aromatic plane induced by insertion of Li atoms [42].

Though the reversible capacity of milled graphite is high, its cycling behavior is usually not satisfactory and capacity fades [28,37,40,42]. This fading is perhaps due to coalescence of edge planes resulting in decrease number of edge planes and the activity of the edge planes by solvents [40]. In addition, the annihilation of some vacancies and microcavities or voids by some removably bound interstitial carbon and the electrolyte penetrating gradually into voids during the Li insertion and desertion process also lead to capacity fading [42].

From the above illustration, the milling should not be too drastic or long in order to get optimal performance in terms of reversible capacity, coulomb efficiency in the first cycle and cycling behavior. If it is too long or drastic, unfavorable effects such as increase in irreversible capacity and decrease in coulomb efficiency will happen [30]. In the case of mildly

Table 4
Effect of the change in particle sizes of graphite anode material by a mechano-chemical method on its reversible lithium capacity

Sample	Average diameter of particle (μm)	Specific surface area (m^2/g)	Active specific surface area (m^2/g)	L_c (nm)	Reversible capacity (mAh/g)
LONZA KS-6	3.34	22	0.44	65	880
LONZA KS-25	10.5	13	0.09	90	550
LONZA KS-44	20.25	10	0.04	100	250

milled graphite samples, the coulomb efficiency is much higher though their reversible capacity is lower, and optimal performance is obtained with a suitable particle size [27,29]. When the particle size of the milled graphite is too big, it cannot deliver high reversible capacity because of the lack of exposure of the edge planes towards the electrolyte. Too fine particle will inevitably incur very big irreversible capacity due to the big surface area [29].

Different atmospheres including air, high purity argon, nitrogen and CO_2 produce different surface chemistry of the milled carbon, which influences the formation of the surface passivating film in electrolyte and therefore the kinetics of the Li insertion process including Li^+ migration through the surface films. The highly reactive carbon sites and the oxygen-containing highly reactive surface groups participate in the formation of the surface film, and do not result in dense films to prevent the exfoliation. As a result, capacity fades [33].

In the case of reactive milling of graphite with lithium, since the surface is lithiated and a bonding between carbon and lithium atoms is developed, insertion compounds with Li/C molar ratios higher than 1/6 (Li/C = 1/6, 1/4 and 1/2) can be prepared [34,45]. They show higher reversible capacities than graphite (372 mA h/g), weaker hysteresis, and smaller irreversible capacities than milled graphite under the same conditions [34]. A primary capacity very close to 1115 mAh/g is observed during the first deintercalation cycle at constant current. The following intercalation–deintercalation cycles yielded capacity close to the theoretical value of 372 mAh/g, typical of natural graphite. Upon immersion of the milled graphite in the electrolyte, a solid electrolyte interface (SEI) is formed spontaneously. Due to the complex nature of the compound prepared by ball milling (a mixture of lithium metal, LiC_3 and LiC_6) the mechanism of the first deintercalation is rather complex. Oxidation of lithium metal happens at about 22 mV versus Li, followed by a decomposition of the superdense phase LiC_3 and LiC_6 at potentials that correspond to the normal electrochemical lithium de-intercalation from LiC_6. Lithium metal in 'LiC_2' is very active and easily reacts with nitrogen to yield α-Li_3N, which irreversibly de-intercalates about 1.8 ± 0.1 lithium before decomposing [45].

As mentioned above, carbon anode materials from nongraphitic carbon also display structural changes after milling. As a result, the electrochemical performance will also change. In the case of petroleum cokes prepared by milling for 12–24 h, when their average particle size is 6–8 μm, they show the best electrochemical characteristics as determined from cyclic voltammogram and cycling test [39].

Ball milling in air of petroleum coke from heat-treatment at 2350 °C with a L_a of about 10 nm, L_c of >60 nm, and d_{002} of 0.3358 nm also presents beneficial effect on the reversible capacity up to $Li_{0.93}C_6$ [31]. By the way, the irreversible capacity loss is also decreased [31].

3.2. Alloy-based anode materials

Alloy-based anode materials emerged in the late of 1970s. However, the problem associated with the growth of dendrite has not been completely overcome. As a result, it gave way to graphitic carbons in the early of 1990s [3]. Recently, it was found that the introduction of a conductor acting as a buffer could lead to an improvement in electrochemical performance. Consequently, novel alloy-based anode materials have become another topic, and mainly include tin-based, silicon-based, and antimony-based alloy anode materials.

3.2.1. Tin-based alloys

Cu–Sn is the first reported novel alloy anode materials since Sn can form alloys with Li up to $Li_{22}Sn_4$ [3,46]. However, it is prepared by chemical reaction. Recently, it was found that Cu–Sn alloys could also be prepared by mechanochemical methods with flake below 1 μm [47]. In comparison with other methods such as gas-atomizing and melt-spinning technique, it shows better electrochemical performance. Similar to Cu–Sn alloys prepared by other methods, the presence of excess Cu in alloy, relative to CuSn, presents improved cyclability at the expense of capacity, whereas an excess of Sn results in poor cyclability with high initial capacity [3,46].

Mechanical mixing of Mg and Sn yields another tin-based alloy, Mg_2Sn. The obtained structure changes with mixing time. A mixture of cubic and orthorhombic phases of Mg_2Sn ensures a good electrochemical performance. After 20 cycles, its reversible capacity is still the range of 250–300 mAh/g as shown in Fig. 2. The main reason is that the interstitial space is mainly responsible for lithium intercalation, and this intercalation will not produce destruction of the phase composition like the alloying of Sn with Li [48]. The capacity of the mixture may be due to the layered structure of orthorhombic phase, and the coexistence of cubic phase decreases the generated internal stress as lithium inserts. As for the cubic Mg_2Sn, although there exist some sites, they appear to be too narrow. On the contrary, the orthorhombic phase has a layered structure and the distance between the layers is enough to accommodate Li atoms, and lithium can insert into the layers [48]. However, another

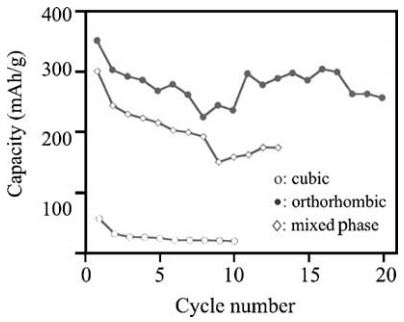

Fig. 2. Dependence of reversible capacity with cycle number on the structure of Mg_2Sn from a mechanochemical method (from ref. [48]).

report says that lithium can alloy with Sn in the Mg_2Sn besides insertion into the Mg_2Sn lattice. As a result, the initial reversible capacity is much higher, 460 mAh/g [49]. Mg in the alloys does not participate in the alloying reaction with Li. In a restricted voltage range, Mg_2Sn shows improved cycling performance due to the prevention of Sn from aggregating into larger clusters [49]. Perhaps it is not crystalline, and further study on this contradiction is needed.

Nanocrystalline Ni–57 mass% Sn and Ni_3Sn_4 alloy can be prepared by high-energy ball milling [50–52], and they show very high initial large discharge capacity of 1515 mAh/g and charge capacity. The irreversible capacity loss happens primarily during the first cycle [52]. However, the capacity fades still continuously after the first cycle, and it is poorer than well-developed nanocrystalline Ni_3Sn_4 from the annealing, wherein lithium atoms reversibly react with tin atoms in the grain boundaries without capacity fading for extended cycling [52].

After intensive ball milling, a composite of graphite and tin is obtained and Sn is encapsulated in the ductile graphite matrix on a nanometer scale. During the milling, graphite becomes amorphous and tin becomes nanocrystalline. In contrast with the ball milling of graphite, the graphite in this composite introduces less interstitial carbon atoms due to the existence of Sn. Tin particles are broken down to 15–20 nm, and still attains an ordered crystalline state. The lithium storage capacity increases with the addition of Sn, which could be attributed to the reaction of Sn with Li to form Li_xSn alloys. The volume expansion due to the alloying process may be buffered by the amorphous graphite matrix. Both Sn and graphite contribute to reversible capacity, which are identified from the charge and discharge peaks, corresponding to 0.5–0.6 V and 0.1 V. The role of interstitial sites such as vacancies and disorganized regions is also displayed in the first cycle as a peak around 1.4 V. Generally, the capacity of the ball-milled C, $C_{0.9}Sn_{0.1}$, and $C_{0.8}Sn_{0.2}$ electrodes decreases with cycling quite quickly, but the $C_{0.9}Sn_{0.1}$ and $C_{0.8}Sn_{0.2}$ electrodes have better cyclability than that of the ball-milled graphite electrode as shown in Fig. 3 [53]. In the meanwhile, it is also better than that of pure Sn, whose volume change can be 67% and may result in serious cracking or crumbling of Li–Sn alloys.

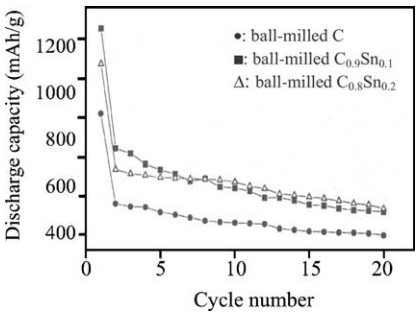

Fig. 3. Change of discharge (intercalation) capacities with cycle number for the ball-milled graphite, $Sn_{0.8}Sn_{0.2}$ and $C_{0.9}Sn_{0.1}$ (from ref. [53]).

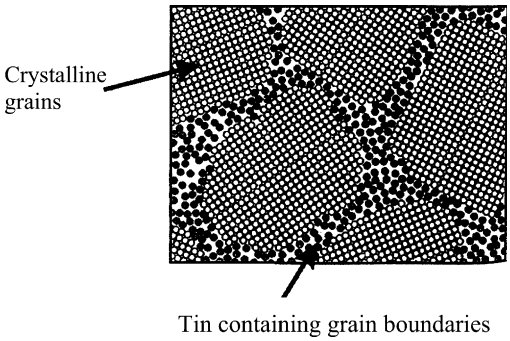

Fig. 4. Nanostructured material showing crystalline grains and atoms in the grain boundaries (from ref. [54]).

Sn-based alloys can be further ball-milled with graphite and produce novel anode materials. For example, in the case of an intermetallic compound, $SnMn_3C$, which has a perovskite structure, is inactive to lithium insertion, after ball milling of Sn, Mn, and C (MCMB) the obtained $SnMn_3C$ comprises of nanostructured particles with different crystallographic orientations, as shown in Fig. 4. The grain boundaries apparently act as channels to allow Li to enter the particles. The lithium atoms then reversibly react with Sn atoms at and within the grain boundaries to deliver a reversible capacity of approximately 150 mAh/g with no capacity loss during cycling [54]. As to other Sn-based alloys such as $SnFe_3C$, it will be similar to $SnMn_3C$ after ball milling. For comparison, some selected results are summarized in Table 5.

In summary, tin-based alloys prepared by mechanochemical methods can be anode materials for lithium ion battery, and their electrochemical performance can be comparable with those from chemical reactions. Of course, the mechanochemical methods affect the structure of the prepared samples, and their electrochemical performance. With further progress, novel tin-based alloy anode materials will appear in combination with other preparation techniques.

3.2.2. *Silicon-based alloys*

Silicon is similar to tin, and can form alloys up to $Li_{22}Si_4$ [3]. As a result, Si-based alloys anode materials are also promising when they are prepared by mechanochemical methods, as shown in Table 5.

SiAg powders formed by the mechanical alloying process appear to contain a uniform dispersion of Si in ductile Ag matrix. Its cycling stability is significantly improved by limiting the cutoff potential. The SiAg electrode prepared by milling for 50 h shows good cyclability with little fade over the first 50 cycles with a stable capacity of approximately 280 mAh/g or 1150 mAh/cm^3 [55]. The Ag not only provides a buffering environment for nano-Si particles but also serves as a conducting matrix. Of course, as shown in Fig. 5, the cycling depends on milling time. Longer milling time, better dispersion of Si in Ag matrix and better cycling performance though lower initial capacity.

Table 5
Selected results of alloy-based anode materials prepared by mechanochemical methods

Precursors	Composition	Structure	Electrochemical performance		References
			Reversible capacity	Cycling	
Cu + Sn	Cu_6Sn_5	Hexagonal structure	200 mAh/g	Good	[47]
Mg + Sn	Mg_2Sn	Cubic + orthorhombic phase	250–300 mAh/g	Good	[48]
		Cubic + orthorhombic phase	460 mAh/g	Good	[49]
Ni + Sn	Ni_3Sn_4	Nanocrystalline	125–200 mAh/g	Good	[52]
Graphite + Sn	Composite such as $C_{0.9}Sn_{0.1}$, $C_{0.8}Sn_{0.2}$	Amorphous graphite + nanocrystalline Sn	400–600 mAh/g	Good	[53]
Sn + Mn + C	$SnMn_3C$	Perovskite, nanoparticles	150 mAh/g	Good	[54]
Si + Ag	SiAg	Nanosized Si in Ag matrix	ca. 280 Mah/g	Good	[55]
Si + TiN		Nanocrystallien or amorphous Si dispersed in TiN	ca. 300 mAh/g	Good	[56]
Ni (Fe) + Si	NiSi (FeSi)	Mixture of NiSi (FeSi) and Si	600–1000 mAh/g	Poor	[57]
Graphite + Si	Composite such as $C_{0.8}Si_{0.2}$		1039 mAh/g	Satisfactory	[59]
$Fe_{80}Si_{20}$ + graphite	Composite		ca. 600 mAh/g	Good	[60]
β-Zn_4Sb_3	ZnSb + unknown structure		Increased to 566 mAh/g	Poor	[62]
Co + Sb	$CoSb_3$	Fine powder, <100 nm	586	Poor	[63]
Zn_4Sb_3 + graphite	Composite		581	Good	[64]

In nanocomposites of silicon and TiN prepared by high-energy mechanical milling, very fine Si particles distribute homogeneously inside the TiN matrix. Si alloys and dealloys with lithium during cycling while TiN remains inactive providing structural stability. A composite containing 33.3 mol% Si obtained after 12 h milling exhibits a stable capacity of about 300 mAh/g. The composites are composed of nanosized TiN containing a uniform dispersion of Si independent of the composition. The very small size of the Si crystals prevents the identification of a distinct phase boundary between Si and TiN. As a result, the volume changes continuously rather than abruptly and discretely. Thus, its influence on the neighboring inactive phase is minimized. As a result, preliminary cycling shows good capacity retention reflecting good phase and microstructural stability [56].

Other nanosize intermetallic alloy powders such as NiSi, FeSi, and $FeSi_2$ can also be prepared by high-energy ball milling [51,57,58]. During lithium insertion into the alloy electrodes, Si acts as active centers, which react with Li to form Li_xSi alloys. A high lithium storage capacity of 1180 mAh/g (7050 mAh/cm^3) is observed for the NiSi electrode, with some irreversibility [57,58]. In the case of nanocrystalline $FeSi_2$, it exhibits a large first discharge capacity of 1129 mAh/g. However, in comparison with the annealed $FeSi_2$, its irreversible capacity is higher and the initial capacity decreases rapidly in the early stage of cycling [51].

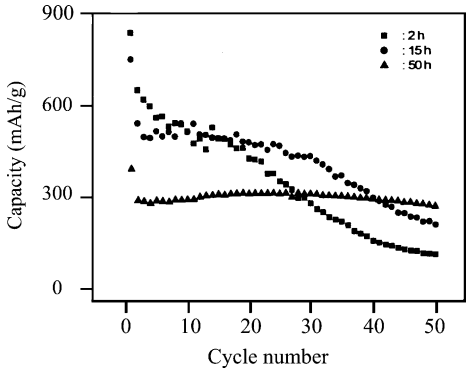

Fig. 5. Cycling behavior SiAg with milling time when cycled between 0.07 and 2.0 V (from ref. [55]).

By the way, other kinds of alloy-based anode materials such as that of Mg with Si [3,55] can also be prepared, and some of them can have a reversible capacity of >500 mAh/g.

Silicon can also form nanocomposite $C_{1-x}Si_x$ ($x = 0$, 0.1, 0.2, 0.25) with graphite by mechanical milling [59]. After ball milling, the crystal size of graphite increases but the size of silicon decreases with the silicon content. Ball-milled $C_{1-x}Si_x$ materials react reversibly with lithium, and the reversible capacity increases from 437 mAh/g in the ball-milled pure graphite to 1039 mAh/g in ball-milled $C_{0.8}Si_{0.2}$ materials. The excess capacity due to the Li extraction from silicon appears at a potential around 0.4 V. After 20 cycles the reversible capacity of $C_{0.8}Si_{0.2}$ is 794 mAh/g. This behavior is due to the fact, that nanosize silicon particles decrease the crumbling rate during Li insertion and extraction [59].

A $Fe_{20}Si_{80}$ alloy electrode delivers large initial capacity, but its capacity degrades rapidly with cycling. When graphite is ball-milled with $Fe_{20}Si_{80}$ to get $Fe_{20}Si_{80}$ alloy–graphite composite, it shows good cycleability and a high reversible capacity of about 600 mAh/g. These composites appear to be promising candidates for anode materials of lithium ion batteries [60].

In summary, mechanochemical methods can prepare Si-based alloys with good electrochemical performance. In comparison with other Si-containing compounds such as pyrolytic carbons from Si-containing polymers [3,61], it is simple in process. In addition, the introduction of –Si–O–

bonds can be avoided. As a result, it is promising to prepare Si-containing anode materials for lithium ion batteries. Presumably, further development will lead to the appearance of novel Si-based alloys with better electrochemical performance.

3.2.3. Antimony-based alloys

Since the chemical properties of Sb are similar to those of Si and Sn and the lithium insertion can arrive at the level of Li_3Sb, Sb-containing alloys can also be potential anodes for lithium ion batteries including β-Zn_4Sb_3, $CoSb_3$ and InSb when they are prepared by mechanochemical methods, as shown in Table 5.

β-Zn_4Sb_3 has a rhombohedric crystal structure with $a = 1.2231$ nm and $c = 1.2428$ nm, and its density (6.077 g/cm^3) is lower than those of Zn (7.14 g/cm^3) and Sb (6.684 g/cm^3), suggesting that there is some space therein for lithium storage.

After high-energy ball milling, β-Zn_4Sb_3 alloy powders change to ZnSb structure together with some other unknown structure. In comparison with the unmilled β-Zn_4Sb_3, the reversible capacity in the first cycle increases from 503 to 566 mAh/g, and the plateau of lithium deinsertion from the alloy decreases from 0.95 to 0.85 V, indicating a lower resistance for lithium ion in the milled samples. However, the cycle stability of the milled β-Zn_4Sb_3 is still obviously not satisfactory. During cycling several lithium-containing compounds such as LiZnSb, Li_3Sb, and LiZn have been formed successively during the insertion of lithium into Zn_4Sb_3 [62].

$CoSb_3$ compounds with different particle size can also be prepared from ball milling of Co and Sb. Of course, the particle size decreases with the ball-milling time and affects the reversible capacity. For example, the reversible capacity in the first cycle increases with the decrease in the particle size of the materials from 385 mAh/g for the coarse powders (about 6 μm) to 586 mAh/g for the ball-milled fine powders (smaller than 100 nm). Though the capacity retention during cycling of the ball-milled samples is poorer than expected because of the granular structures, after 50 cycles its volume reversible capacity still remains higher than 1600 mAh/cm^3, which is almost twice that of graphite [63].

On the basis of $CoSb_3$, Fe can be incorporated by high-energy ball milling. During lithium insertion into the obtained ultrafine $CoFe_3Sb_{12}$ powders, lithium forms Li_3Sb alloy with Sb therein. The reversible capacity in first cycle is 396 mAh/g [64].

In the case of InSb from ball milling, it is found that when $x \leq 0.27$, there is a reversible reaction between InSb and Li as shown in the following:

$$x\mathrm{Li} + \mathrm{InSb} \Leftrightarrow \mathrm{Li}_x\mathrm{InSb} \quad (x \leq 0.27) \tag{1}$$

When $x > 0.27$, the reaction of the following will happen:

$$3\,\mathrm{Li} + \mathrm{InSb} \rightarrow \mathrm{Li}_3\mathrm{Sb} + \mathrm{In} \tag{2}$$

the voltage plateau of this process is above 0.65 V, and the cycling behavior is good. At lower potential, the produced In reacts with Li and forms alloy of $InLi_x$. At this stage, the cycling is poor [65]. Perhaps at the first stage, In can act as a buffer to resist the crack or volume expansion.

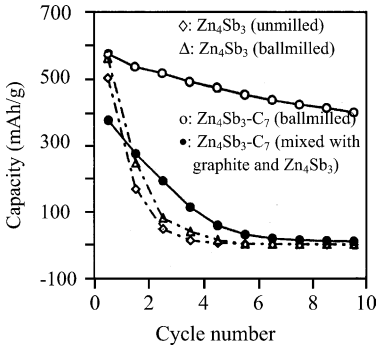

Fig. 6. Capacity of unmilled and milled Zn_4Sb_3, Zn_4Sb_3–C_7 and the mixture of Zn_4Sb_3 and graphite with cycle number (from ref. [62]).

In order to improve its cycling behavior of Sb-based alloys, graphite can also be added further therein as a buffer and a conductive matrix similar to the composite of Sn and Si with graphite [53,60]. For example, a composite material $CoFe_3Sb_{12}$–C_{16} from ball milling of $CoFe_3Sb_{12}$ and graphite shows superior cycling even at large current density of 100 mA/g [64]. A composite of Zn_4Sb_3–(C_7) prepared by milling Zn_4Sb_3 with graphite shows better cycling behavior, whose lithium ion extraction capacity at the first cycle is 581 mAh/g and at 10th cycle is still 402 mAh/g [62,66]. From the comparison of electrochemical performance of unmilled, milled Zn_4Sb_3 and the composite Zn_4Sb_3–(C_7) as shown in Fig. 6, the composite possesses high initial reversible capacity, small voltage hysteresis, and good capacity retention, which makes this material an interesting anode material for lithium ion batteries [66]. When about 11.8 wt.% graphite is added during ball milling, the reversible capacity of the composite of Zn_4Sb_3 and graphite in the first cycle increases from 507 to 580 mAh/g.

Of course, other kinds of metals can also form alloys with Sb by mechanochemical reactions if they present good conductivity and good stability during cycling.

3.3. Other kinds of anode materials

Other kinds of anode materials mainly include tin-based oxides. The system SnO–B_2O_3–P_2O_5 is the first reported one [3,67]. It was at first prepared by calcination. Now amorphous materials in the system SnO–B_2O_3–P_2O_5, with or without the addition of Li_2O, can be synthesized by mechanical milling treatment of oxides in a dry N_2 atmosphere at room temperature. These materials, obtained as fine powders of SnO–B_2O_3–P_2O_5, are comprised of fine particles smaller than 1 μm in diameter and secondary particles of the aggregates of this fine particles. They present discharge capacities in the first cycle more than 500 mAh/g at a constant current of 1.5 mA/cm^2. The capacities for Li_2O added materials are comparable or slightly larger than that for the

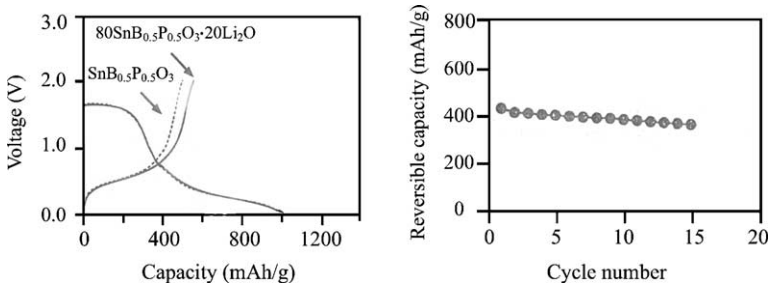

Fig. 7. (a) Discharge and charge curves in the first cycle for amorphous materials of $SnB_{0.5}P_{0.5}O_3$ and $80SnB_{0.5}P_{0.5}O_3{\cdot}20Li_2O$ after mechanical milling for 100 h; and (b) cycling behavior of $80SnB_{0.5}P_{0.5}O_3{\cdot}20Li_2O$ between 0 and 0.8 V (from reference [68]).

materials without the addition of Li_2O as shown in Fig. 7(a). Charge–discharge curves of these materials are similar to those for the glassy powders in the system $SnO–B_2O_3–P_2O_5$ prepared by a melt quenching procedure [68]. By selecting the cutoff voltage, good cycling is achieved as shown in Fig. 7(b).

Of course, other kinds of metals or metal oxides can also be doped to obtain an improvement in electrochemical performance [2]. For example, Mo-doped $Sn_{1-x}Mo_xO_2$ mixed oxides of low crystallinity have been synthesized by mechanical milling of the starting elements in an air atmosphere at room temperature, and they are solid solutions with a cassiterite-type structure with Mo in the tetravalent oxidation state. The addition of Mo has two favorable effects, namely: (a) it increases the discharge capacity and (b) it improves capacity retention in cells cycled between 1.0 and 0.0 V. The formation of a Li–Mo–O oxide conductive matrix during the electrochemical insertion of lithium may account for this enhanced performance, and the silica present in the samples originating from the agate jar and balls of milling apparatus plays a minor role based on the stability of the Si–O bond [69].

Zinc doped tin oxides with different ratios are prepared by ball milling of ZnO and SnO_2, and it is found that individual ball milling of the oxides increase the capacity, co-milling is fairly neutral and ball milling before solid-state reaction presents a detrimental effect on electrochemical performance [70].

The research reviewed above is mainly directed at the cycling behavior of tin-based oxides. However, there is another major problem, i.e. the large irreversible capacity in the first cycle. In order to decrease the irreversible capacity, ball milling with different compounds such as Li_2O, SiO, and Li_3N is a good choice.

Nanocomposites of lithium oxide and tin are prepared by ball milling and the tin particles are uniformly distributed within a lithium oxide matrix with the majority of the tin particles on the order of 100 nm or less. As a result, during cycling, chemical reduction of SnO is avoided since Sn exists in metallic state [71].

Amorphous $50SiO{\cdot}50SnO$ (mol%) powders are synthesized by mechanical milling treatment of starting materials SiO and SnO in a dry N_2 atmosphere at room temperature. The resultant powders show a high capacity over 800 mAh/g at the potential range of 0–2.0 V versus Li^+/Li with a current density of 1.5 mA/cm^2. This first discharge capacity of amorphous $50SiO{\cdot}50SnO$ powders is much larger than that of amorphous materials in the system $SnO–B_2O_3–P_2O_5$ obtained by mechanical milling reported previously. In addition, its irreversible capacity is smaller than that of the latter [72].

Ball milling of SnO with Li_3N produces the mixture of Li_2O and Sn, wherein Sn is homogeneously distributed, and its particle size is about 100 nm or lower. During the first cycle, the irreversible capacity is greatly decreased since Li_3N reacts with SnO during the milling process as the following (3) [73].

$$2Li_3N + 3SnO \rightarrow 3Li_2O + 3Sn + 3N_2 \uparrow \quad (3)$$

Since irreversible capacity can be decreased greatly, and the cycling behavior can be improved by introduction of other elements, tin-based oxides from mechanical milling are promising candidates as anode materials for lithium ion batteries.

The mechanochemical methods can prepare composite oxides with the same structure and composition as solid-state reactions at high temperature, and they show promise to decrease irreversible capacity of oxide anode materials.

4. Solid electrolytes

Solid electrolytes include inorganic and solid polymer electrolytes [3]. The latter is usually prepared by polymerization. Of course, mechanochemical methods are also applied in its preparation such as the addition of nanofillers [3,74]. However, it is not the main or determining process, and this aspect will not be expounded here. The former usually include sulfides and oxides. In the application in lithium ion batteries, it should be amorphous or non-crystalline. As a result, mechanochemical methods like milling or grinding are a promising way to prepare inorganic solid electrolytes [3].

So far, the main materials prepared by mechanochemical methods are amorphous sulfide and oxysulfide glasses [3,75]. Based on crystal Li_2S and SiS_2, grinding for 20 h

produces an amorphous glass $60Li_2S{\cdot}40SiS_2$ (mol%). Its conductivity at room temperature is about 10^{-4} S/cm, completely comparable with that from melt quenching, and the transport number of Li^+ is nearly 1.0 [76]. In the case of the amorphous mixture of Li_2S and P_2S_5 the result is the same [77]. In addition, the amorphous region is extended in comparison with that of samples from melt-quenching, and the molar ratio of Li_2S in amorphous $xLi_2S{\cdot}(1-x)P_2S_5$ can be high up to 0.80 [77].

Li_2O, SiO_2, P_2O_5, and GeO_2 can also be doped during mechanochemical processes to prepare amorphous inorganic electrolytes [78,79]. For example, the amorphous solid electrolyte of $(100-x)(0.6Li_2S{\cdot}0.4SiS_2){\cdot}xLi_4SiO_4$ shows an ionic conductivity above 10^{-4} S/cm. Between $x = 0$ and 5, its conductivity is the highest [78]. The oxysulfide amorphous materials in the systems $95(0.6Li_2S{\cdot}0.4SiS_2){\cdot}5Li_xMO_y$ (M = Si, P and Ge) exhibit high conductivity over 10^{-4} S/cm at room temperature, a lithium transport number of unity, and a wide potential window of 10 V [79]. During milling, the particle size decreases at first with milling period, and later increases because the particles aggregate with each other [78]. The local structure of the mechanically milled amorphous materials containing Li_4SiO_4 is similar to that of the corresponding melt-quenched glasses, in which the SiS_4 and $SiOS_3$ tetrahedral units are mainly present. SiO_nS_{4-n} ($n = 1$, 2, 3) tetrahedral units are formed in the case of the addition of Li_4SiO_4 and Li_4GeO_4 to the base sulfide system, while these units are not present in the addition of Li_3PO_4. The reactivity of Li_xMO_y derived from its basicity affects the structure and formation process of the oxysulfide materials prepared by mechanical milling [79].

LiI can also be doped into the sulfides by mechanochemical techniques. The ionic conductivity of pressed pellets of the 0.17 B_2S_3–0.37 Li_2S–0.46 LiI vitreous powder is at the optimal value when a large grain size (70 μm) powder is pressed at 12 t/cm^2. The highest relative density obtained is 0.93. Long grinding period leads to partial crystallization and, as a consequence, a decrease in conductivity and an increase in activation energy [80].

When these kinds of amorphous sulfides and oxysulfides are used as electrolyte and built into solid lithium ion batteries, they exhibit excellent cycling performance [78,79]. For example, an all-solid-state battery fabricated with $LiCo_{0.3}Ni_{0.7}O_2$ fine powder as the cathode material, the glass $60Li_2S{\cdot}40SiS_2$ (mol%) as the solid electrolyte, and a metallic indium foil as the anode shows a rechargeable capacity of 98 mAh/g based on the cathode material, and its cycle efficiency is almost 100% after the second cycle [81].

5. Concluding remarks

In conclusion, mechanochemical methods are promising to prepare materials for lithium ion batteries. Compared with conventional solid-state reaction, the mechanochemical methods appear to accelerate and simplify the synthesis process and decrease the energy expenses as well as the cost of the materials. Furthermore, the prepared materials also present good electrochemical performance. For example, cathode materials such as $LiMn_2O_4$ spinels present better cycling behavior due to the highly disordered nanocrystallines which can accommodate the Jahn-Teller distortions. Carbonaceous anode materials such as graphite show very high capacity due to the introduction of a lot of defects such as voids/nanocavities, and the change into nanoparticles. In the case of alloy-based anode materials, their cycling behavior is also improved since heteroatoms can be homogeneously incorporated into the prepared nanocomposites and buffer the drastic volume change. The prepared solid glass electrolytes also show high conductivity (>10^{-4} S/cm), and the fabricated true solid-state lithium ion battery presents good cycling behavior. Further research of the actions of different kinds of mechanochemical methods on the change of the prepared amorphous materials during cycling is needed.

In addition, they can also be used to prepare novel materials for lithium ion batteries such as particulate-reinforced Al/SiC composite anode material [82], nanoanode composites composed of Li_2O/M and Li_2S/M (M = Co, Fe) [83], which show good cycling behavior.

Furthermore, mechanochemical methods can be applied to prepare materials for lithium ion batteries in combination with other techniques. For example, a superionic crystal analogous to highly conductive thio-LISICON is first successfully prepared by mechanically milling Li_2S–P_2S_5 glasses following crystallization at high temperature. The formed superionic crystal enhances the conductivity of the glass, which can be around 10^{-3} S/cm at ambient temperature for the glass–ceramics derived from the Li-rich $80Li_2S{\cdot}20P_2S_5$ (mol%) glass [77,84]. Grinding followed by a firing at 400 °C or more can prepare spinel $Li_4Mn_5O_{12}$ with pure phase, which is difficult to obtain just by heat-treatment [85]. Combination of wet ball milling and rotating can prepare pure $LiMn_2O_4$ spinel with a uniform particle size distribution and excellent cycling [86].

References

[1] C. Suryanarayana, Prog. Mater. Sci. 46 (2001) 1, and references therein.
[2] V.V. Volkov, K.G. Myakishev, Inorg. Chim. Acta 289 (1999) 51, and references therein.
[3] Y.P. Wu, C. Wan, C. Jiang, S.B. Fang, Lithium ion secondary batteries, Beijing, Chemical Industry Press, 2002.
[4] Y.P. Wu, E. Rahm, R. Holze, Electrochim. Acta 47 (2002) 3491.
[5] Y.P. Wu, E. Rahm, R. Holze, Chin. J. Power Sources 27 (2003) 45.
[6] Y.P. Wu, E. Rahm, R. Holze, Chin. J. Batteries (Dianchi) 32 (2002) 256.

[7] A. Manthiram, J. Kim, Recent. Res. Dev. Electrochem. 2 (1999) 31.
[8] Y.P. Wu, E. Rahm, R. Holze, Chin. J. Power Sources 27 (2003) 260.
[9] Y.P. Wu, E. Rahm, R. Holze, S.B. Fang, J. Solid State Electrochem., in press.
[10] J.M. Fernandez-Rodriguez, J. Morales, J.L. Tirado, React. Solids 4 (1987) 163.
[11] W.T. Jeong, K.S. Lee, J. Alloys Compd. 322 (2001) 205.
[12] N.V. Kosova, V.F. Anufrienko, T.V. Larina, A. Rougier, L. Aymard, J.M. Tarascon, J. Solid State Chem. 165 (2002) 56.
[13] H.W. You, H.Y. Lee, S.W. Jang, K.C. Shin, S.M. Lee, J.K. Lee, S.J. Lee, H.K. Baik, D.S. Rhee, J. Mater. Sci. Lett. 17 (1998) 931.
[14] N.V. Kosova, NATO Science Series, II: Mathematics, Physics and Chemistry, vol. 61, New Trends in Intercalation Compounds for Energy Storage, 2002, p. 507.
[15] W.T. Jeong, K.S. Lee, J. Power Sources 104 (2002) 195.
[16] M.N. Obrovac, O. Mao, J. Dahn, Solid State Ionics 112 (1998) 9.
[17] M.M. Thackeray, Prog. Solid State Chem. 25 (1997) 1.
[18] N.V. Kosova, I.P. Asanov, E.T. Devyatkina, E.G. Avvakumov, J. Solid State Chem. 146 (1999) 184.
[19] N.V. Kosova, N.F. Uvarov, E.T. Devyatkina, E.G. Avvakumov, Solid State Ionics 135 (2000) 107.
[20] H.J. Choi, K.M. Lee, G. Kim, J.G. Lee, J. Am. Ceram. Soc. 84 (2001) 242.
[21] S. Soiron, A. Rougier, L. Aymard, J.M. Tarascon, J. Power Sources 97/98 (2001) 402.
[22] S. Kang, J. Goodenough, L. Rabenberg, Chem. Mater. 13 (2001) 1758.
[23] S. Kang, J. Goodenough, L. Rabenberg, Electrochem. Solid-State Lett. 4 (2001) A49.
[24] N.V. Kosova, E.T. Devyatkina, S.G. Kozlova, J. Power Sources 97/98 (2001) 406.
[25] A. Andersson, B. Kalska, P. Eyob, D. Aernout, L. Haggstrom, J.O. Thomas, Solid State Ionics 140 (2001) 63.
[26] Y.P. Wu, S.B. Fang, Y.Y. Jiang, Solid State Ionics 120 (1999) 117.
[27] F. Disma, L. Aymard, L. Dupont, J.M. Tarascon, J. Electrochem. Soc. 143 (1996) 3959.
[28] C. Park, S.M. Oh, J. Korean Electrochem. Soc. 2 (1999) 221.
[29] H. Wang, T. Ikeda, K. Fukuda, M. Yoshio, J. Power Sources 83 (1999) 141.
[30] C. Natarajan, H. Fujimoto, A. Mabuchi, K. Tokumitsu, T. Kasuh, J. Power Sources 92 (2001) 187.
[31] R. Kostecki, T. Tran, X. Song, K. Kinoshita, F. McLarnon, J. Electrochem. Soc. 144 (1997) 3111.
[32] T.S. Ong, H. Yang, J. Electrochem. Soc. 149 (2002) A1.
[33] D. Aurbach, B. Markovsky, A. Nimberger, E. Levi, Y. Gofer, J. Electrochem. Soc. 149 (2002) A152.
[34] P. Azais, L. Duclaux, A. Faugere, F. Beguin, Appl. Phys. Lett. 81 (2002) 775.
[35] F. Salver-Disma, C. Lenain, B. Beaudoin, L. Aymard, J. Tarascon, Solid State Ionics 98 (1997) 145.
[36] K. Matsubara, T. Katsuramaki, K. Kawamura, T. Ema, Tanso 175 (1996) 249.
[37] F. Salvern-Disma, A. Rouzaud, J. Pasquier, J. Tarascon, J. Lasseguer, J. Power Sources 81/82 (1999) 291.
[38] T.S. Ong, H. Yang, Carbon 38 (2000) 2077.
[39] H. Kim, C. Lee, Kongop Hwahak 9 (1998) 781.
[40] T. Ema, A. Kitahara, Japan Patent, JP 8-213020 (1996).
[41] L. Aymard, F. Disma, J. Tarascon, US 6,066,413 (2000).
[42] C. Wang, G. Wu, W. Li, J. Power Sources 76 (1998) 1.
[43] T. Norio, O. Takahasa, T. Toshio, N. Hideyuki, K. Yasushi, EP Appl EP 675555 (1995).
[44] D.G. Fauteux, US Patent US 5,512,392 (1996).
[45] R. Tossici, R. Janot, F. Nobili, D. Guerard, R. Marassi, Electrochim. Acta 48 (2003) 1419.
[46] M.M. Thackeray, J.T. Vaughey, A.J. Kahaian, K.D. Kelper, R. Benedek, Electrochem. Comm. 1 (1999) 111.
[47] Y. Xia, T. Sakai, T. Fujieda, M. Wada, H. Yoshinaga, J. Electrochem. Soc. 148 (2001) A471.
[48] H. Sakauchi, H. Maeta, M. Kubota, H. Honda, T. Esaka, Electrochemistry 68 (2000) 632.
[49] H. Kim, Y.J. Kim, D.G. Kim, H.J. Sohn, T. Kang, Solid State Ionics 144 (2001) 41.
[50] J.H. Ahn, Y.J. Kim, G. Wang, M. Lindsay, H. Liu, S. Dou, Mater. Trans. 43 (2002) 63.
[51] J. Ahn, G. Wang, H. Liu, S. Dou, Materials Science Forum, vol. 360–362, Metastable, Mechanically Alloyed and Nanocrystalline Materials, 2001, p. 595.
[52] H.Y. Lee, S.W. Jang, S.M. Lee, S.J. Lee, H.K. Baik, J. Power Sources 112 (2002) 8.
[53] G. Wang, J. Ahn, M. Lindsay, L. Sun, D. Bradhurst, S. Dou, H. Liu, J. Power Sources 97/98 (2001) 211.
[54] L. Beaulieu, D. Larcher, R. Dunlap, J. Dahn, J. Electrochem. Soc. 147 (2000) 3206.
[55] S. Hwang, H. Lee, S. Jang, S. Lee, S. Lee, H. Baik, J. Lee, Electrochem. Solid-State Lett. 4 (2001) A97.
[56] I. Kim, P. Kumta, G. Blomgren, Electrochem. Solid-State Lett. 3 (2000) 493.
[57] G. Wang, L. Sun, D. Bradhurst, S. Zhong, S. Dou, H. Liu, J. Power Sources 88 (2000) 278.
[58] G. Wang, L. Sun, D. Bradhurst, S. Zhong, S. Dou, H. Liu, J. Alloys Compd. 306 (2000) 249.
[59] C. Wang, G. Wu, X. Zhang, Z. Qi, W. Li, J. Electrochem. Soc. 145 (1998) 2751.
[60] H.Y. Lee, S.M. Lee, J. Power Sources 112 (2002) 649.
[61] A.M. Wilson, G. Zank, K. Eguchi, W. Xing, J. Dahn, J. Power Sources 68 (1997) 195.
[62] G. Cao, X. Zhao, T. Li, C. Lu, J. Power Sources 94 (2001) 102.
[63] L. Zhang, X. Zhao, X. Jiang, G. Cao, Cailiao Yanjiu Xuebao 16 (2002) 429.
[64] X. Zhao, L. Zhang, G. Cao, C. Lu, B. Zhou, Cailiao Yanjiu Xuebao 15 (2001) 469.
[65] K.C. Hewitt, L.Y. Beaulieu, J. Dhan, J. Electrochem. Soc. 148 (2001) A402.
[66] X. Zhao, G. Cao, Electrochim. Acta 46 (2001) 891.
[67] Y. Idota, T. Kubota, A. Matsufuji, Y. Maekawa, T. Miyasaka, Science 276 (1997) 1395.
[68] H. Morimoto, M. Nakai, M. Tatsumisago, T. Minami, J. Electrochem. Soc. 146 (1999) 3970.
[69] M. Martos, J. Morales, L. Sanchez, J. Mater. Chem. 12 (2002) 2979.
[70] F. Belliard, P.A. Connor, J. Irvine, Ionics 5 (1999) 450.
[71] D. Foster, J. Wolfenstine, J. Read, W. Behl, in: Proceedings of the 39th Power Sources Conference, 2000, p. 89.
[72] H. Morimoto, M. Tatsumisago, T. Minami, Electrochem. Solid-State Lett. 4 (2001) A16.
[73] D. Foster, J. Wolfenstine, J. Read, W. Behl, Electrochem. Solid-State Lett. 3 (2000) 203.
[74] F. Croce, B.B. Appetecchi, L. Persi, B. Scrosati, Nature 394 (1998) 456.
[75] M. Tatsumisago, J. Ceram. Soc. Jpn. 109 (2001) 809.
[76] H. Morimoto, H. Yamashita, M. Tatsumisago, T. Minami, J. Am. Ceram. Soc. 82 (1999) 1352.
[77] M. Tatsumisago, S. Hama, A. Hayashi, H. Morimoto, T. Minami, Solid State Ionics 154/155 (2002) 635.
[78] R. Komiya, A. Hayashi, H. Morimoto, M. Tatsumisago, T. Minami, Solid State Ionics 140 (2001) 83.
[79] A. Hayashi, H. Yamashita, M. Tatsumisago, T. Minami, Solid State Ionics 148 (2002) 381.
[80] M. Makyta, A. Levasseur, P. Hagenmuller, Mater. Res. Bull. 19 (1984) 1361.

[81] N. Machida, H. Maeda, H. Peng, T. Shigematsu, J. Electrochem. Soc. 149 (2002) A688.
[82] G. Jeong, Y. Kim, H. Sohn, T. Kang, J. Power Sources 101 (2001) 201.
[83] M. Obrovac, J. Dahn, Electrochem. Solid-State Lett. 5 (2002) A70.
[84] H. Akitoshi, H. Shigenori, M. Tsutomu, T. Masahiro, Electrochem. Commun. 5 (2003) 111.
[85] Y. Tanaka, Q. Zhang, F. Saito, Powder Technol. 132 (2003) 74.
[86] G. Song, Y. Zhou, W. Zhou, Wuji Cailiao Xuebao 16 (2001) 486.